First-Principles Study of Thermodynamic Properties in Thin-Film Photovoltaics

by

Jon R. Tucker

A Thesis Presented in Partial Fulfillment
of the Requirements for the Degree
Master of Science

Approved October 2011 by the
Graduate Supervisory Committee:

Mark Van Schilfgaarde, Chair
Nathan Newman
James Adams

ARIZONA STATE UNIVERSITY

December 2011

ABSTRACT

This thesis focuses on the theoretical work done to determine thermodynamic properties of a chalcopyrite thin-film material for use as a photovoltaic material in a tandem device. The material of main focus here is $ZnGeAs_2$, which was chosen for the relative abundance of constituents, favorable photovoltaic properties, and good lattice matching with $ZnSnP_2$, the other component in this tandem device. This work is divided into two main chapters, which will cover: calculations and method to determine the formation energy and abundance of native point defects, and a model to calculate the vapor pressure over a ternary material from first-principles.

The purpose of this work is to guide experimental work being done in tandem to synthesize $ZnGeAs_2$ in thin-film form with high enough quality such that it can be used as a photovoltaic. Since properties of photovoltaic depend greatly on defect concentrations and film quality, a theoretical understanding of how laboratory conditions affect these properties is very valuable. The work done here is from first-principles and utilizes density functional theory using the local density approximation. Results from the native point defect study show that the zinc vacancy (V_{Zn}) and the germanium antisite (Ge_{Zn}) are the more prominent defects; which most likely produce non-stoichiometric films. The vapor pressure model for a ternary system is validated using known vapor pressure for monatomic and binary test systems. With a valid ternary system vapor pressure model, results show there is a kinetic barrier to decomposition for $ZnGeAs_2$.

TABLE OF CONTENTS

Page

LIST OF TABLES . . . iv

LIST OF FIGURES . . . v

CHAPTER

1 Introduction . . . 1

1.1 Density Functional Theory (DFT) . . . 1

Thomas-Fermi Model . . . 1

Hohenberg-Kohn theorem . . . 2

Kohn-Sham Method . . . 3

Local Density Approximation (LDA) . . . 3

Full-Potential Linear Muffin Tin Orbital (FP-LMTO) method . . . 4

1.2 Thermodynamics From First-Principles . . . 4

Partition Functions . . . 4

Chemical Equilibrim . . . 6

2 Native Point Defect Study . . . 8

2.1 Introduction . . . 8

2.2 Defect Formation . . . 9

Calculation of Formation Energies . . . 9

Chemical Potential Limits . . . 10

2.3 Defect Concentrations . . . 12

2.4 Computational Methods . . . 13

2.5 Results . . . 14

Defect Formation Energy . . . 14

Defect Concentrations . . . 17

2.6 Conclusions . . . 20

3 *ab initio* Vapor Pressure Model . . . 22

3.1 Introduction . . . 22

CHAPTER Page

3.2 Methods . . . 23

Ideal monatomic gas . . . 24

Diatomic Gas . . . 25

Debye model of solid . . . 26

Debye frequency . . . 26

Solid partition function . . . 28

3.3 Single component system: Zn, Ge, Sn . . . 29

3.4 Binary system: GaAs . . . 30

3.5 Ternary system: $ZnGeAs_2$ . . . 31

Free energy minimization . . . 32

3.6 Results and Discussion . . . 33

Monatomic Systems: Zn, Ge, Sn . . . 33

Binary System: GaAs . . . 36

Ternary System: $ZnGeAs_2$ . . . 37

3.7 Conclusions . . . 39

4 Summary . . . 40

4.1 Native Point Defects in $ZnGeAs_2$ . . . 40

4.2 *ab initio* Vapor Pressure Model . . . 41

REFERENCES . . . 42

APPENDIX . . . 45

A Differentiation of Solid Partition Function . . . 46

LIST OF TABLES

Table — Page

2.1 Electronic contribution to native point defect formation energy in neutral charge state using Eq. 2.2 14

2.2 Heats of formation for various materials and compounds, calculated from DFT 15

2.3 Neutral native point defect formation energies at points labeled in Fig. 2.1 with corresponding chemical potentials. All values are in electron volts. 16

3.1 Materials data used for calculation of Zn, Ge, and Sn vapor pressures 34

3.2 Materials data used for calculations of GaAs vapor pressure 36

LIST OF FIGURES

Figure | Page

2.1 Stability diagram showing allowed ranges for Zn and Ge chemical potentials to form $ZnGeAs_2$ (area bounded by lines AB, BD, and DC). . 15

2.2 Defect formation energy of native cation defects along the line line that would run through points B and D on Fig. 2.1, i.e. $\mu_{Zn} - \mu_{Ge}$ 17

2.3 Defect concentrations as a function of (total) pressure at various temperatures. The pressure ranges are calculated from the chemical potentials for Zn and Ge according to a line extending from the origin of Fig. 2.1 to the point on the line BD where $\mu_{Zn} = \mu_{Ge}$. 18

2.4 Defect concentrations as a function of (total) pressure at various temperatures. The pressure ranges are calculated from the chemical potentials for Zn and Ge according to a line running through points B and D on Fig. 2.1. This plot follows the same chemical potential conditions as in Fig. 2.2 where the chemical potential of As is zero. 19

3.1 Arrhenius plots of the comparison between experimental data [Mar67] and theory (LDA and PBE calculations) for the monatomic systems A) Zn, B) Sn, C) Ge, and the binary system D) GaAs 35

3.2 Arrhenius plot of the vapor pressure over ZGA in comparison to thermal decomposition data, the vapor pressure over liquid ZGA at the melting point [SW75], and arrival rates for Zn and As via sputtering [SG84] and As via MBE synthesis [STP89] 38

Chapter 1

Introduction

This chapter will provide a brief summary of the foundations used throughout this work. The first two sections will cover the methods behind the calculation of material properties from first-principles using the density functional theory. The remainder of the chapter will focus on a few properties used to calculate thermodynamic properties in conjunction with density functional theory, which will be a short introduction to statistical mechanics. The information in this introductory chapter is primarily from the following reference books: [PY89, Kub65, Rei65, Cal60].

1.1 Density Functional Theory (DFT)

To predict the electronic structure of matter the problem involves the solution of a complicated many-body problem . The purpose of the density functional theory is to replace a complex wave function that is a function of each particles' position vector, $\Psi(\mathbf{x_1}, \mathbf{x_2}, ..., \mathbf{x_n})$, with the much simpler election density $n(\mathbf{r})$, hence where the name density functional theory originates. This section will cover a brief summary outlining the principles of density functional theory (DFT).

Thomas-Fermi Model

The Thomas-Fermi model is the predecessor to DFT and it allows for the replacement of the complicated wave function mentioned above with the simpler electron density $n(\mathbf{r})$. Thomas and Fermi realized that the distribution of electrons can be approximated by statistical methods. Thomas in 1927 stated that "Electrons are distributed uniformly in the six-dimensional phase space for the motions of an electron at the rate of two for each h^3 of volume" and that there is an is an effective potential field that "is itself determined by the nuclear charge and this

distribution of electrons." [PY89] Another break through for this approximation is the use of local relations approximated as a homogeneous electron gas to the electronic properties of a system. This is also know as the local density approximation and is very important to DFT. The main result from the Thomas-Fermi model is a way to calculate the kinetic energy from the electron density:

$$T_{TF}\left[n\right] = C_F \int n^{5/3}\left(\mathbf{r}\right) d\mathbf{r} \tag{1.1}$$

The total energy of an atom can then be expressed as:

$$E_{TF}\left[n\left(\mathbf{r}\right)\right] = C_F \int n^{5/3}\left(\mathbf{r}\right) d\mathbf{r} - Z \int \frac{n\left(\mathbf{r}\right)}{\mathbf{r}} d\mathbf{r} + \frac{1}{2} \iint \frac{n\left(\mathbf{r}_1\right) n\left(\mathbf{r}_2\right)}{\left|\mathbf{r}_1 - \mathbf{r}_2\right|} d\mathbf{r}_1 d\mathbf{r}_2 \tag{1.2}$$

Where the first term is the kinetic energy, the second is the repulsion from the ion cores, and the third is the electron-electron interaction term. The equation for the total energy of at atom depends only on the electron density. The downside to this equation however is that it neglects any exchange and correlation terms and breaks down with molecules (predicts no bonding).

Hohenberg-Kohn theorem

While the Thomas-Fermi model provides a good foundation for modern DFT, it was not validated until Hohenberg and Kohn provided their two theorems – the existence theorem and variational theorem.

Theorem 1 – existence theorem: the external potential $V'_{ext}\left(r\right)$ is determined, within a trivial additive constant, by the electron density $n\left(\mathbf{r}\right)$.

This theorem provides the direct mapping of the external electron potential $V'_{ext}\left(r\right)$ to the electronic density for the ground state of a many electron system

Theorem 2 – variational theorem: for a trail density $\tilde{n}\left(\mathbf{r}\right)$, such $\tilde{n}\left(\mathbf{r}\right) \geq 0$ and $\int \tilde{n}\left(\mathbf{r}\right) d\mathbf{r} = N$,

$$E_0 \leq E_{V_{ext}}\left[\tilde{n}\right] \tag{1.3}$$

This theorem establishes the variational principle for DFT, which states that ground state density minimizes the electronic energy of the system.

Kohn-Sham Method

In the Thomas-Fermi model and other similar methods approximations are made for the electron density and potential, and there are difficulties going beyond these approximations. Kohn and Sham invented an indirect approach for the kinetic energy term which turned DFT into a practical tool. They did this by introducing orbitals so that the kinetic energy can be calculated to good accuracy. Kohn and Sham set up the problem such that the kinetic energy, $T[n]$, is exact. The total energy equation under Kohn and Sham then becomes:

$$E[n] = T_S[n] + J[n] + E_{xc}[n] + \int V_{ext}(\mathbf{r})\, n(\mathbf{r})\, d\mathbf{r} \tag{1.4}$$

The advantage of this method is that by separating out the kinetic energy term, $T[n]$, and the long range Hartree interactions the remaining exchange-correlation term, $E_{xc}[n]$ can be approximated. The actual $E_{xc}[n]$ should be very complex, but progress has been made in achieving accurate approximations. Another advantage of this method is that it can be solved iteratively to self convergence.

Local Density Approximation (LDA)

With the Kohn-Sham method a way to calculate the kinetic energy accurately is possible, the remaining difficulty remains in the exchange-correlation term, this is where the local density approximation (LDA) is useful. In the Thomas-Fermi model local uniform electron gas was used to calculate the kinetic energy. However, this is not needed now with the Kohn-Sham method, in the LDA the local uniform electron gas is used for the exchange-correlation part of the energy functional. The local density approximation for the exchange-correlation energy

is:

$$E_{xc}^{LDA} = \int n(\mathbf{r})\, \epsilon_{xc}(n)\, d\mathbf{r} \tag{1.5}$$

This method is applicable for systems where the electron density varies slowly over a de broglie wavelength and it becomes exact in the limit of a slowly varying density. It becomes less useful in systems with strong energy gradients, due to directional bonding, which is known to systematically overbind. Corrections and approximations have been made to improve the accuracy of LDA such as the PBE method [PBE96].

Full-Potential Linear Muffin Tin Orbital (FP-LMTO) method

The calculations performed here for the total energies heavily rely on the FP-LMTO method; a computational implementation of DFT and the LDA. Its main advantage is the use of augmented smooth Hankel functions for the basis set to reduce computation time. This method uses atom-centered basis functions of well-defined angular momentum, constructed out of Hankel functions, as well as augmentation to introduce atomic detail into the basis functions in the vicinity of each nucleus [MvSC00]. This method uses a more complex basis set, which happens to reduce computation time due to the reduced basis size.

1.2 Thermodynamics From First-Principles

Partition Functions

To calculate macroscopic thermodynamic properties from microscopic properties (or first-principles) the methods of statistical mechanics are used. The partition function is a key part of statistical mechanics. If it is known many physical properties (e.g. energy, pressure, entropy) can be calculated from having various derivatives. In statistical mechanics a near-universal method for the calculation

of macroscopic properties is to evaluate the partition function [Rei65]:

$$Z = \sum_r e^{-\beta E_r} \tag{1.6}$$

This is an unrestricted sum, and if one knows all particles in the system, as well as their interactions, it is possible to calculate this sum by knowing the quantum states of the system. This however, is only possible for simple systems such as an ideal gas. When moving beyond simple systems the mathematics become extremely complex.

An important property of the partition function is the additivity of the energy which leads to a simple product of partition functions when calculating multiple noninteracting or weakly interacting systems. This is particularly useful when performing calculations involving a gas phase with multiple species that can be treated as an ideal gas. Using equation 1.6 the energy of a system is the derivative of the natural log of the partition function:

$$E_r = \frac{\partial lnZ}{\partial \beta} \tag{1.7}$$

If the system consists of two states, the energy of the system is simply the sum of the two states:

$$E = E_i + E_j \tag{1.8}$$

The partition function of the system then becomes:

$$Z = \sum_{i,j} e^{-(E_i+E_j)\beta} = \sum_{i,j} e^{-E_i\beta} e^{-E_j\beta} = \left(\sum_i e^{-E_i\beta}\right)\left(\sum_j e^{-E_j\beta}\right) = Z_i Z_j \tag{1.9}$$

When taking the natural log to derive the energy from the partition function, it becomes a sum:

$$lnZ = lnZ_i + lnZ_j \tag{1.10}$$

Which leads back to the initial assumption that the energy of the system is a sum of the subsystems. Thus, two important properties of the partition function that will be used here are the sum of energy states, and product of subsystem partition functions (Eqs. 1.8 and 1.9).

For a system consisting of N particles that is thermally isolated the most probable configuration is the one in which entropy is maximized, i.e.:

$$S(E_1, V_1, N_1; E_2, V_2, N_2; ...; E_j, V_j, N_j) = max \tag{1.11}$$

where

$$S = S_1(E_1, V_1, N_1) + S_2(E_2, V_2, N_2) + ... + S_j(E_j, V_j, N_j) \tag{1.12}$$

which leads to the condition that

$$dS = dS_1(E_1, V_1, N_1) + dS_2(E_2, V_2, N_2) + ... + dS_j(E_j, V_j, N_j) = 0 \tag{1.13}$$

where

$$dS_j = \frac{1}{T_j}dE_j + \frac{p_j}{T_j}dV_j - \frac{\mu_j}{T_j}dN_j \tag{1.14}$$

where T_j is the temperature, p_j is the pressure, and μ_j is the chemical potential of each species. Satisfying the maximization of entropy thus leads to the conditions for chemical equilibrium:

$$T_1 = T_2 = ... = T_j \tag{1.15}$$

$$p_1 = p_2 = ... = p_j \tag{1.16}$$

$$\mu_1 = \mu_2 = ... = \mu_j \tag{1.17}$$

If the system is constructed in such a way that the temperatures and pressures of the components are equal, then one only needs to be concerned with satisfying the third condition in Eq. 1.17. For a general chemical reaction, $n_a A + n_b B \rightarrow n_c C$, the condition for chemical equilibrium can be written as:

$$\sum_j n_i \mu_i = 0 \tag{1.18}$$

where the coefficients on the products are taken to be positive, and those on the reactants are taken to be negative. By using this equilibrium condition one can calculate the number of atoms in a particular phase.

As mentioned previously, if one knows the partition function of the system then all thermodynamic properties can be calculated from it. The chemical potential, μ_j of each component, which is defined as:

$$\mu_j = \frac{\partial F_j}{\partial N_j} \tag{1.19}$$

can be calculated from the partition function. The free energy, F_j, of a component in terms of the partition function is defined as:

$$F_j = -k_b T ln Z_j \tag{1.20}$$

Thus the chemical potential can be written in terms of the partition function as well:

$$\mu_j = -k_b T \frac{\partial ln Z_j}{\partial N_j} \tag{1.21}$$

By using Eqs. 1.18, 1.21, and the correct partition function the number of atoms in a particle phase can be calculated from first principles.

Chapter 2

Native Point Defect Study

2.1 Introduction

The chalcopyrite material $ZnGeAs_2$ is a group II-IV-V semiconductor that has been selected as a candidate for inclusion in a high efficiency tandem photovoltaic thin-film device. There have been reports of $ZnGeAs_2$ films with mobilities in excess of 50 cm^2/V-sec [SG84, CCO+87, STP89] as well as minority carrier lifetimes of approximately 150 ns [TB98]. When including this material in a tandem cell design with $ZnSnP_2$, there is good lattice matching, and ideal band gaps (1.15eV and 1.65eV respectively). Additionally all constituents are naturally abundant. With these favorable properties, $ZnGeAs_2$ appears to be a very ideal compound for photovoltaic devices, however the synthesis of this material is not simple.

Synthesis of high quality thin-films of $ZnGeAs_2$ is primarily difficult due to the high volatility of the Zn and As species. There have been a number of reports indicating the growth of $ZnGeAs_2$ films are possible, but typically the conditions are non-ideal, or there is a very narrow growth window. Shah and Greene [SG84] have reported growth of single crystal $ZnGeAs_2$ films by sputtering using substrate temperatures of 450-520°C with additional evaporation of Zn and As_4 increasing over-pressures to 1mTorr. Under these growth conditions almost none of the Zn and As was incorporated into the film. Molecular beam epitaxy has also been used [CCO+87] with substrate temperatures of 380°C, but was only able to achieve a growth rate of 50 nm/h. It is apparent that the synthesis of $ZnGeAs_2$ requires precise control over growth conditions as well as additional insight to the factors that are limiting growth.

It is proposed that the difficulties with the synthesis of $ZnGeAs_2$ films can be explained by the formation of native defects, which can be controlled

by adjusting growth parameters. There have been theoretical studies performed [ZWZKY98, JML05, BvSS94] which detail the calculation of defect formation energies and their possible effects on material properties. The goal here is to follow a similar approach to determine most abundant native defects as a function of laboratory conditions that may hinder the synthesis of stoichiometric $ZnGeAs_2$ thin-films. This study will cover the use of density functional theory for the calculation of defect formation energies and defect densities from first-principles.

2.2 Defect Formation

Calculation of Formation Energies

A supercell approach has been taken here for the calculation of defect formation energies in $ZnGeAs_2$, using a supercell that consists of 128 atoms. Large atomic systems are required for defect formation calculations to negate the effects of the cell boundaries on the distortion as a result of the defect. A similar study carried out by Jiang et. al. [JML05] on $ZnGeP_2$ used a 64 atom cell which was sufficient in performing defect formation calculations. Here it is assumed that a 128 atom supercell will provide an ideal level of accuracy, while not being overly computationally expensive.

The defect formation energy is calculated by taking the perfect 128 atom supercell and adding the defect to be studied, which in this case included the three vacancies (V_{Zn}, V_{Ge}, V_{As}) and the two cation anti-sites (Ge_{Zn}, Zn_{Ge}). It is assumed these are the primary defects that will effect the ability to grow stoichiometric photovoltaic quality thin-films. The formation energy of a neutral (q=0) defect α in $ZnGeAs_2$ is dependent on the chemical potentials [ZWZKY98]:

$$\Delta H_f(\alpha, q=0) = \Delta E(\alpha, q=0) + n_{Zn}\mu_{Zn} + n_{Ge}\mu_{Ge} + n_{As}\mu_{As} \tag{2.1}$$

where

$$\Delta E(\alpha, q=0) = E(\alpha, q=0) - E(ZnGeAs_2) + n_{Zn}\mu_{Zn}^{solid} + n_{Ge}\mu_{Ge}^{solid} + n_{As}\mu_{As}^{solid} \tag{2.2}$$

In Eq. 2.1, n_i are the atomic species that are either added or removed from the systems, and μ_i are the chemical potentials of the atomic species, which are controlled by laboratory conditions (pressure and temperature). Eq. 2.2 is the expression for the difference in energy between the defect cell ($E(\alpha, q = 0)$) and the perfect cell ($E(ZnGeAs_2)$). These energies are obtained from density functional theory calculations (DFT) of fully relaxed supercells. The n_i terms are the same as in Eq. 2.1, the solid chemical potentials, μ_i^{solid}, are the total energies of the elemental solids, which are also obtained from DFT calculations. Also using statistical mechanics, the chemical potentials of the elemental species can be shown as a function of pressure and temperature.

Chemical Potential Limits

The chemical potentials in Eq. 2.1 are bound by the conditions where precipitation of the solid elements will occur:

$$\mu_{Zn} \leq 0, \qquad \mu_{Ge} \leq 0, \qquad \mu_{As} \leq 0 \tag{2.3}$$

Another boundary placed on the chemical potentials is the formation of the stable $ZnGeAs_2$ compound:

$$\mu_{Zn} + \mu_{Ge} + 2\mu_{As} = \Delta H_f(ZnGeAs_2) \tag{2.4}$$

where $\Delta H_f(ZnGeAs_2)$ is the formation energy of $ZnGeAs_2$ calculated from DFT. These two conditions can be used to form a stability diagram, which is similar to a phase diagram, in that it displays where a certain compound, in this case $ZnGeAs_2$ is stable as a function of chemical potential. With only these two boundary

conditions the diagram would be a simple triangle when plotted in 2-D (one potential is set as zero, typically the anion).

In $CuInSe_2$, another chalcopyrite material, it was determined that there is a range of compounds that can exist [ZWZKY98] inside the conditions set by Eqs. 2.3 and 2.4. The wide range of possible stoichiometric compounds existing for this material was attributed to the formation of a defect complex which has a low energy of formation. In another similar study conducted for $ZnGeP_2$ [JML05], it was determined that the same was not true for this chalcopyrite compound, and that there were only two other possible compounds that could form inside the stability triangle. Since the material of focus here ($ZnGeAs_2$) and $ZnGeP_2$ are both II-IV-V compounds, it was assumed they would be more similar, and therefore it was assumed the stability diagram of $ZnGeAs_2$ would be similar as well. The stability diagram of $ZnGeAs_2$ was constructed in a similar manner to $ZnGeP_2$, and it was found that the compounds Ge_3As_4 and Zn_3As_2 could also exist within the boundaries of the stability diagram.

This then imposes the additional boundary conditions to the stability region:

$$3\mu_{Zn} + 2\mu_{As} \leq \Delta H_f(Zn_3As_2) \tag{2.5}$$

$$3\mu_{Ge} + 4\mu_{As} \leq \Delta H_f(Ge_3As_4) \tag{2.6}$$

Using the conditions for the chemical potentials such that the elemental species do not precipitate, $ZnGeAs_2$ forms a stable compound, and Ge_3As_4 and Zn_3As_2 do not form, a stability diagram can be constructed for this system. The construction of a stability diagram allows for the calculation of defect formation energies over only the conditions under which synthesis of a stable $ZnGeAs_2$ compound is possible.

2.3 Defect Concentrations

The quasichemical formulation [Kro74] will be followed here for the calculation of defect densities as a function of laboratory parameters. The primary focus here will be to determine the abundance of native point defects which are charge neutral for guidance in the synthesis of $ZnGeAs_2$ thin-films. The calculations of defect formation energies described above will be used here as well since the defect densities are a function of the formation energy.

A similar study has been performed on the pseudobinary alloy $Hg_xCd_{1-x}Te$ [BvSS94], which will be the basis for this study. This system however differs in that it must be treated as a ternary system, not as a binary alloy, due to the fixed stoichiometry and the strict adherence to the specific cation (A and B) and anion (C) sublattices in the chalcopyrite structure ABC_2. In this system there are three components (A, B, and C), and two phases (solid and vapor) – to stay in accordance with Gibbs's phase rule there must be three degrees of freedom.

Typically in binary systems there are two degree's of freedom which can include temperature, chemical potential, and pressure. The degrees of freedom chosen are temperature, chemical potential, and stoichiometry. Temperature is a very natural degree of freedom to control as it translates directly to experiment. Chemical potential has been selected due to the formulation of the defect formation energy in Eq. 2.1, and with the use of statistical mechanics can be expressed as a function of temperature and pressure. Stoichiometry has been chosen because the goal is to synthesize a stoichiometric $ZnGeAs_2$ thin-film device, and it is therefor of interest to control this parameter.

In the quasichemical approximation the law of mass action is used to determine the density of non-interacting defects at small densities [Kro74]:

$$K_{X^x} = \theta \exp\left(-\frac{F_{X^x}}{k_B T}\right) = [X^x] \tag{2.7}$$

where F^x is the formation energy of the neutral defect X, with density $[X^x]$. The term θ is the number of unit cells per volume to convert the result to defects per volume. The formation energy, F_{X^x} is a sum of vibrational, electronic, translational, and a degeneracy contributions:

$$F_{X^x} = F_X^{vib} + F_X^{el} + F_X^{trans} + k_B T ln(G) \tag{2.8}$$

The electronic term (F_X^{el}) is the defect formation energy calculated from DFT using Eq. 2.1, which also includes the translational term (F_X^{trans}) in the form of the chemical potentials. Here it has been decided to ignore the vibrational term which is a common practice as the electronic contribution tends to be the dominant term, and it is assumed the vibrational contribution will not have a major impact on this study. The degeneracy term, which accounts for the degeneracy of the reactants, is take from the quasichemical approximation. For a reaction $A+B \rightarrow C+D$ the degeneracy G is equal to $(g_C g_D)/(g_A g_B)$, where g_i is the degeneracy of reactant i.

2.4 Computational Methods

The total energy calculations that were performed to determine defect formation energies utilized density functional theory (DFT) with the local density approximation [HK64, KS65]. Total energy calculations were performed using a 128-atom super cell with a 4x4x4 mesh of k points, to calculate the vacancy formation energy of the three atomic species. The defect super cell was relaxed using the full-potential (FP) linearized muffin-tin orbital (LMTO) method [MvSC00], on a 2x2x2 k point mesh.

2.5 Results

Defect Formation Energy

The calculated defect formation energies (Eq. 2.2) for charge neutral native point defects in $ZnGeAs_2$ are listed in Table 2.2, along with the corresponding atom exchanges to and from the vapor phase. A positive value signifies an atom moving from the solid to vapor, with a negative representing the transfer from the gas reservoir to the solid. For example, in the creation of a Zn_{Ge} anti-site, a germanium atom is first moved from the solid to the vapor ($+n_{Ge}$), then the vacant site is occupied by the zinc atom from the vapor ($-n_{Zn}$).

Table 2.1: Electronic contribution to native point defect formation energy in neutral charge state using Eq. 2.2

Defect	F_x^{elec} [eV]	n_{Zn}	n_{Ge}	n_{As}
V_{Zn}	1.866	+1	0	0
V_{Ge}	2.645	0	+1	0
V_{As}	3.310	0	0	+1
Zn_{Ge}	0.478	-1	+1	0
Ge_{Zn}	1.288	+1	-1	0

While the Zn_{Ge} anti-site defect has the smallest electronic contribution, it may not be the most abundant defect or have the lowest formation energy, which also contains a contribution from the vapor phase reservoir. To determine the range of chemical potentials to focus on for the calculation of the defect formation energies a stability diagram of the $ZnGeAs_2$ system, Fig. 2.1, has been constructured according to the conditions outlined in Eqs. 2.4, 2.5, and 2.6. The heats of formation required to determine the boundaries of the stability diagram can be found in Table 2.2.

Without using a stability diagram it would be difficult to calculate the formation energies of defects as a function of chemical potentials in regions where

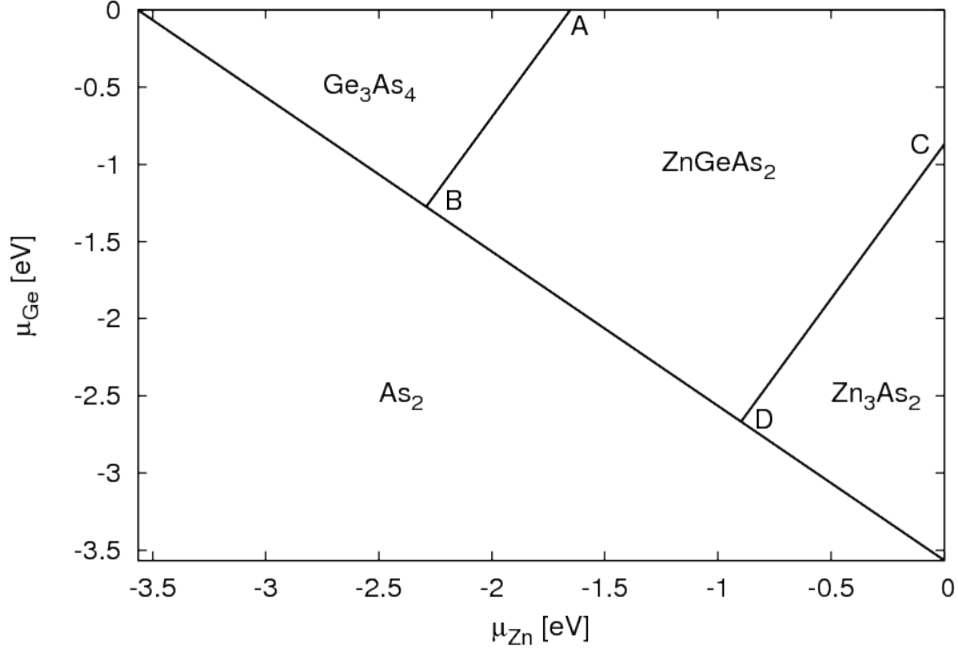

Figure 2.1: Stability diagram showing allowed ranges for Zn and Ge chemical potentials to form $ZnGeAs_2$ (area bounded by lines AB, BD, and DC).

Table 2.2: Heats of formation for various materials and compounds, calculated from DFT

Material	ΔH_f [eV]	Compound	$\Delta H_f [eV]$
Zn (s)	-1.847	$ZnGeAs_2$	-3.565
Ge (s)	-4.468	Ge_3As_4	-3.824
As (s)	–2.449	Zn_3As_2	-2.694

it is possible to synthesize pure $ZnGeAs_2$. From this diagram four points where the various phase lines intersect, have been labeled and the corresponding values can be found in Table 2.3. Also it is important to note on this diagram that as the chemical potential of either Zn or Ge becomes more negative this is indicative of reducing the abundance of the constituent. For example, at the origin where both chemical potentials are zero, this would be a region of Zn and Ge abundance, where as if you were to move down the y-axis towards more negative values for the Ge chemical potential these conditions would be come Ge deficient.

Table 2.3: Neutral native point defect formation energies at points labeled in Fig. 2.1 with corresponding chemical potentials. All values are in electron volts.

	A	B	C	D
μ_{Zn}	-1.635	-2.290	0	-0.898
μ_{Ge}	0	-1.275	-0.871	-2.667
V_{Zn}	0.231	-0.424	1.866	0.968
V_{Ge}	2.645	1.370	1.774	-0.022
Zn_{Ge}	2.115	1.495	-0.391	-1.289
Ge_{Zn}	-0.347	0.273	2.159	3.057

The line BD has been chosen as an area to study the defect formation energy for the defects listed in Table 2.3 as it is a region that will have sufficient amount of As_2 gas present ($\mu_{As} = 0$), and it will show the effects of altering the Zn and Ge compositions. In the experimental work [VTT+11] done in tandem with this research, the difficulty has been to synthesize films with the correct 1:1:2 ratio of Zn, Ge, and As respectively. While there have been some samples grown to be near stoichiometric, the majority have been Ge rich and Zn/As deficient. It is therefor probable that film growth is occurring under conditions of sufficient or excess Ge with Zn deficiencies.

In Fig. 2.2 the formation energies for the four native cation defects are plotted as a function of chemical potential. The range of chemical potentials used for the formation energies falls along the diagonal line running through points B and D in Fig 2.1. The conditions mentioned above (Zn deficient, Ge rich) would fall to the left side of this plot. Based on the defect formation energies here it would appear that the zinc vacancy, V_{Zn} and the anti-site Ge_{Zn}, have the lowest formation energies. These energies also appear to be negative under conditions of increasing Zn deficiency. It would therefor be likely that these two defects are present under current growth conditions which result in Zn deficient films. With the anti-site having such a low (negative under some conditions) formation energy this is likely the cause of off-stoichiometry films.

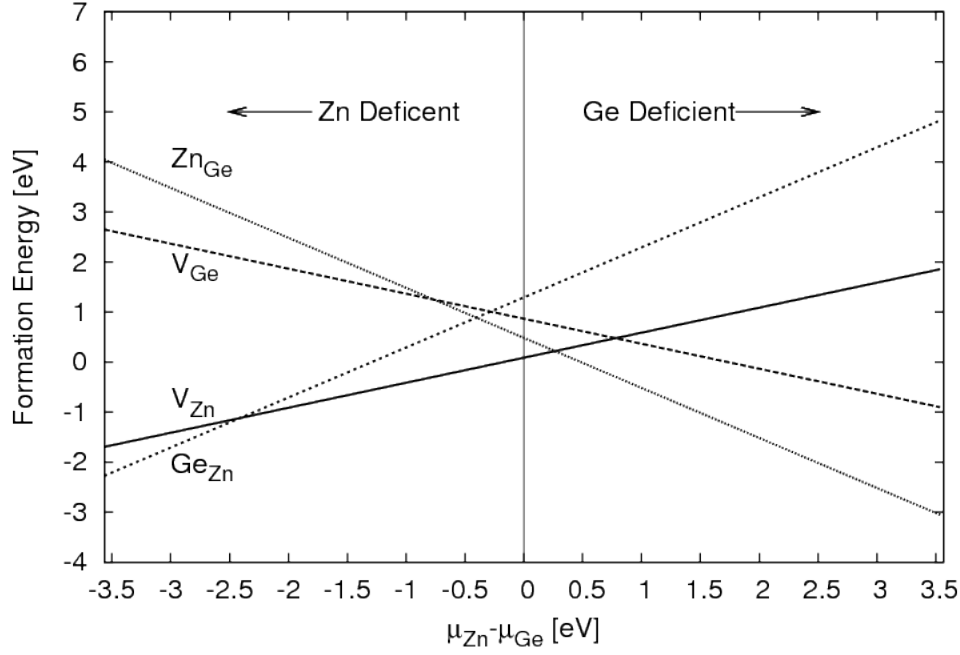

Figure 2.2: Defect formation energy of native cation defects along the line line that would run through points B and D on Fig. 2.1, i.e. $\mu_{Zn} - \mu_{Ge}$

Defect Concentrations

Using the information gained from the defect formation energy calculations the concentrations of these defects as a function of temperature and pressure have been calculated as well in Fig. 2.3. Several plots have been made at temperatures that span typical $ZnGeAs_2$ synthesis conditions. The pressure values were derived from the chemical potentials which contribute the translational formation energy term. The defect concentrations were calculated at the pressures that would result in chemical potentials for Zn and Ge that would fall along a line that runs from the origin in Fig. 2.1 to a point on the line BD where the Zn and Ge chemical potentials are equal. The chemical potential for As if fixed by the stability condition from Eq. 2.4. The temperatures are held constant in each situation. Using these

conditions, the plots will represent the conditions that might occur during normal growth.

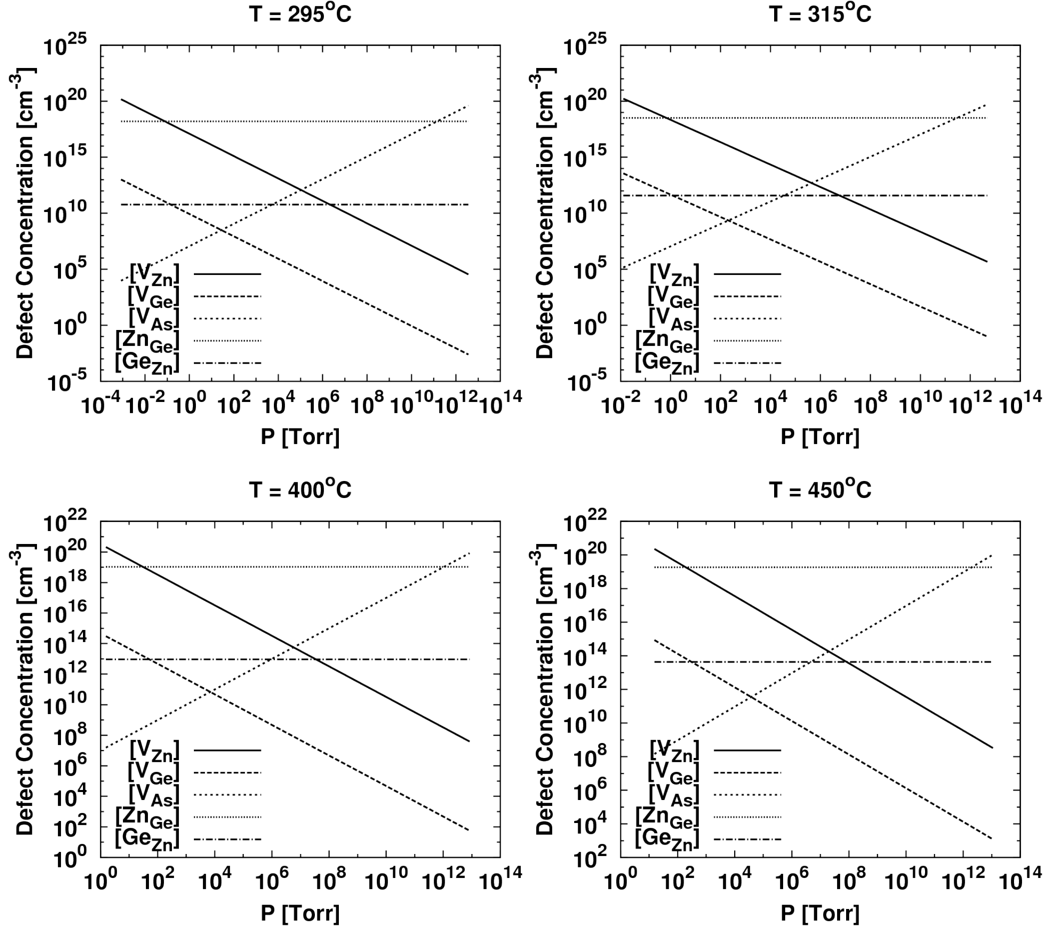

Figure 2.3: Defect concentrations as a function of (total) pressure at various temperatures. The pressure ranges are calculated from the chemical potentials for Zn and Ge according to a line extending from the origin of Fig. 2.1 to the point on the line BD where $\mu_{Zn} = \mu_{Ge}$.

From Fig. 2.3 it is apparent that the two most abundant defects, as predicted by the formation energies in Fig. 2.2, will be the zinc vacancy, V_{Zn} and the Zn_{Ge} anti-site. While there are conditions where the As vacancy would be abundant, these are at extremely high Zn and Ge pressures, which would be extremely low As pressures.

The defect concentration plots generated here only represent a small region of possible growth or annealing conditions. As stated before these conditions were derived from the stability diagram by following a line that would run from the origin to the midpoint on the line running through points B and D. This was done so that all the degrees of freedom could be met, which in this case fixed the chemical potentials of Zn and Ge gases to be equal.

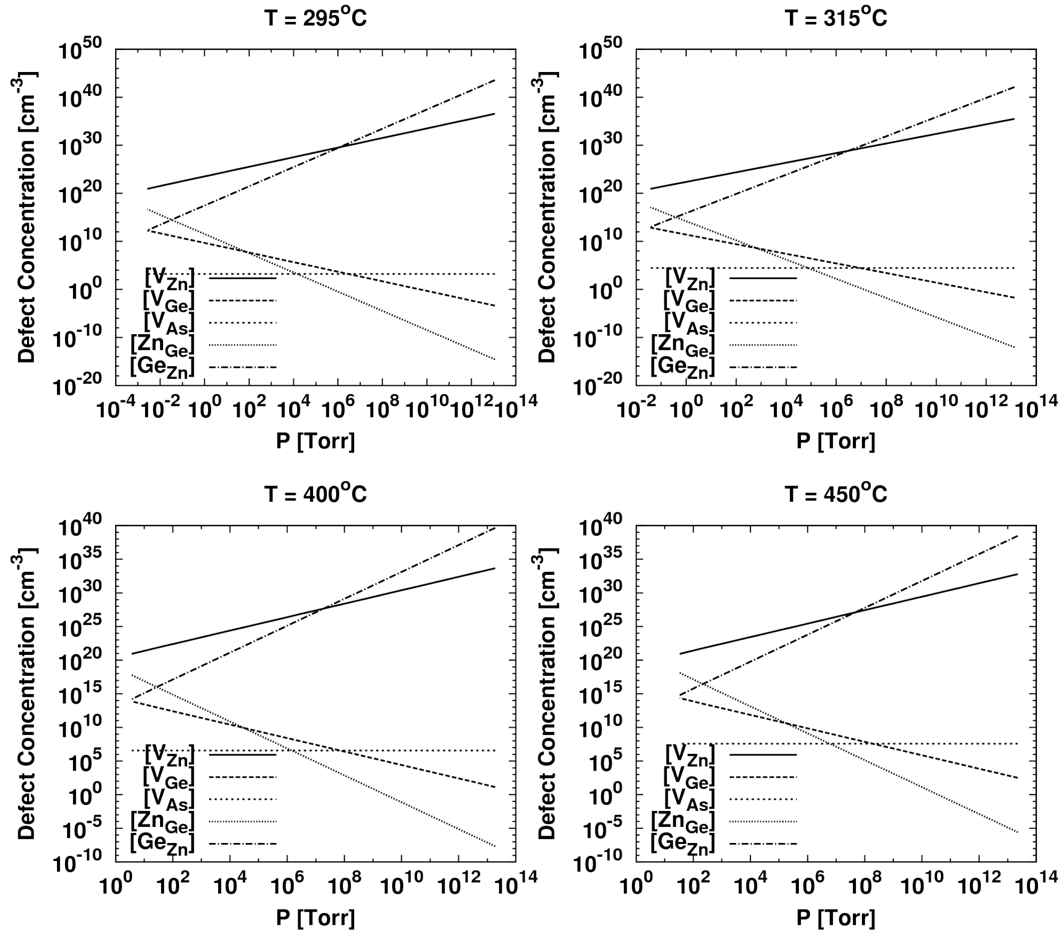

Figure 2.4: Defect concentrations as a function of (total) pressure at various temperatures. The pressure ranges are calculated from the chemical potentials for Zn and Ge according to a line running through points B and D on Fig. 2.1. This plot follows the same chemical potential conditions as in Fig. 2.2 where the chemical potential of As is zero.

For defect concentrations that would most likely be more indicative of typical growth conditions – Ge rich and Zn deficient – Fig. 2.4 was generated by following chemical potential conditions that would occur along a line running through points B and D in Fig. 2.2. In this figure one can see that the most abundant defects appear to be the zinc vacancy, V_{Zn} and the Ge_{Zn} anti-site. This can be explained by the fact that, by moving along a line starting under Zn rich/Ge deficient (Point D) and moving towards point B, the partial pressure of Zn decrease, and Ge increases. This would explain an increase in Zn vacancies, and with addition Ge present, it is likely they will occupy the vacant Zn sites. This could explain the reason for Ge rich films, where growth conditions may be Ge rich and Zn deficient, or at least enough to cause a deviation from stoichiometry.

The two plots shown here only represent a small portion of the possible growth conditions that may occur. By following the methods outlined here one could readily generate addition plots for different growth conditions, or possible annealing profiles. These plots could be very useful tools in performing analysis of growth or annealing conditions to eliminate (or increase) the concentration of certain defects.

2.6 Conclusions

In conclusion, methods for the calculation of defect formation energies and the prediction of defect concentrations have been shown. In calculating the defect formation energies of native point defects in $ZnGeAs_2$ a stability diagram was created from the limits imposed on chemical potentials of the various species. From this the range of chemical potentials to focus on the ranges that would translate to typical growth conditions. Using the range of chemical potentials gained from the stability diagram the formation energy for the two cation vacancies and anti-sites was calculated and plotted. From this it was shown that the zinc vacancy

(V_{Zn}) and the germanium anti-site (Ge_{Zn}) have the lowest formation energies, and should therefore be the most abundant.

To gain a better idea of the abundance of these defects the concentrations for the three vacancies (Zn, Ge, and As) and two anti-sites (Ge_{Zn} and Zn_{Ge}) were calculated. These were thought to be the most likely to contribute to forming off-stoichiometry films, and it was found that under typical growth conditions the zinc vacancy (V_{Zn}) and the germanium anti-site (Ge_{Zn}), would be the most abundant, as predicted from their formation energies. While it appears that under normal growth conditions it may be difficult to limit their formation, the information gathered here could be used to formulate annealing procedures to reduce the native defects in as-grown films. To gain additional knowledge of the defect physics occurring in $ZnGeAs_2$ it would be useful to perform these calculations for ionized defects to gain information for n/p-type doping as well as the possibility of defect complexes that may form.

Chapter 3

ab initio Vapor Pressure Model

3.1 Introduction

$ZnGeAs_2$ has been identified as a promising material for the implementation of a thin-film tandem photovoltaic device. This material has been chosen for several reasons, which include hole mobilities in excess of 50 cm^2/V-sec [SG84, CCO+87, STP89], minority lifetimes of approximately 150 ns [TB98], as well as consisting of relatively abundant materials. Additionally when paired with $ZnSnP_2$ in a tandem design, there is ideal lattice matching between the two species. There, however, has not been widespread synthesis and use of $ZnGeAs_2$ thin-films which is likely due to the high volatility of Zn and As species.

To incorporate two volatile materials at high temperatures and achieve the quality of films needed for photovoltaic applications, growth conditions must be precisely controlled. There is most likely a narrow window of ideal growth conditions that must be maintained, and knowledge of these conditions would greatly improve device synthesis. $ZnGeAs_2$ is a II-IV-V chalcopyrite material, which is tetrahedrally coordinated, and is very similar in structure to III-V zincblende materials (e.g. GaAs). This system contains a cation A and B sublattice, as well as a anion C sub lattice (i.e. ABC_2), any deviation from this could have device killing effects on the system, as seen in the As anti-site in GaAs. This only amplifies the need to determine the window of growth in order to achieve stoichiometry, limited defects, and crystalline films.

The goal of this work has been to develop a model for the calculation of the equilibrium vapor pressure over $ZnGeAs_2$, while working closely with experimental material synthesis. With a vapor pressure diagram for this system much needed insight can be gained towards the determine of the growth process such as

thermodynamic and kinetic limits. This work is unique in that the vapor pressure model described here has been designed from first principles, and should be adaptable to similar systems. The difficulty with developing this model was largely due to the additional degrees of freedom that arise in a ternary system as a result of Gibb's phase rule.

The basis for this model is a statistical mechanic approach adapted from a monatomic vapor pressure model [Kub65]. The approach taken here was to adapt the monatomic model to a ternary system that could account for the additional complexity of the ternary system. The chemical equilibrium of the system was viewed to be a function of competing defect formations which would lead to an exchange between solid and vapor phases. Defect formation energies were calculated using supercell density functional theory (DFT) calculations.

The procedure here was to first validate the use of the monatomic model by using known experimental values of the vapor pressure for Zn, Ge, and Sn solids. Once this model had been validated, the binary system GaAs was then studied using a modified version of this model for binary systems. With a successful model for monatomic and binary systems the model was then developed for the ternary system $ZnGeAs_2$, which is compared to experimental results that were closely coupled with the theory outlined here.

This paper will outline the methods and theory used starting with the monatomic test systems, adaptations for use with a binary system, and finally the development of a ternary model. Results from these methods will be compared and discussed to show the validation of this model.

3.2 Methods

Calculation of macroscopic thermodynamic properties using statistical mechanics of a system at some temperature T (i.e. it is in contact with some heat reservoir),

requires that only the partition function, Z, needs to be known. Once the partition function is known thermodynamic quantities can be readily calculated by taking derivatives of the partition function. The most general expression for the partition function is the sum over all states of the system [Rei65]:

$$Z = \sum_j e^{-\beta E_j}, \quad (\beta = 1/k_B T) \tag{3.1}$$

If one knows the state of all particles in the system, e.g. an ideal non-interacting gas, the partition function can be readily calculated. Difficulties arise in more complex systems, when there are interactions between the particles such as in solids and liquids. Here the partition functions that will be used for an ideal monatomic gas, diatomic gas, and solid are formulated and discussed.

Ideal monatomic gas

The simplest case is the ideal monatomic gas consisting of N_g molecules with mass m contained within a volume V. The total energy of this system is:

$$E = \sum_{j=1}^{N_g} \frac{\mathbf{p}_j^2}{2m} + U(\mathbf{r}_1, \mathbf{r}_2, ..., \mathbf{r}_{N_g}) \tag{3.2}$$

Where $\mathbf{p}_j$ is the momentum of each particle, and U is the interaction energy between each particle. Using this total energy of the system the partition function of the gas can be written as:

$$Z = \frac{1}{h^{3N}} \int e^{-(\beta/2m)\mathbf{p}_1^2} ... \int e^{-(\beta/2m)\mathbf{p}_N^2} d^3\mathbf{p}_N \int e^{-\beta U(\mathbf{r}_1, \mathbf{r}_2, ..., \mathbf{r}_N)} d^3\mathbf{r}_1 ... d^3\mathbf{r}_N \tag{3.3}$$

The kinetic energy is a sum of the terms for each particle and the corresponding part in the partition function becomes a product of N_g integrals, which have the form:

$$\frac{1}{h^3} \int e^{-(\beta/2m)\mathbf{p}^2} d^3\mathbf{p} \tag{3.4}$$

Also because this is a system of non-interacting particles, the interaction energy $U(\mathbf{r}_1, \mathbf{r}_2, ..., \mathbf{r}_N)$, can be set to zero. The exponential in the integration over the

interaction term then goes to one, and the integral is simply equal to the volume, V:

$$\int e^{-\beta U(\mathbf{r}_1,\mathbf{r}_2,\ldots,\mathbf{r}_N)} d^3\mathbf{r}_1 \ldots d^3\mathbf{r}_N = \int d^3\mathbf{r}_1 \ldots d^3\mathbf{r}_N = V^N \quad (3.5)$$

Performing these two integrals for one particle results in the partition function for a single particle:

$$z_g(T,V) = V\left(\frac{2\pi m}{h^2\beta}\right)^{3/2} \quad (3.6)$$

The total partition function of a N_g particle system can then be written as:

$$Z_g(T,V,N_g) = \frac{z_g(T,V)^{N_g}}{N_g!} \quad (3.7)$$

This form of the monatomic gas partition function will be used for calculation of thermodynamic properties.

Diatomic Gas

The diatomic gas partition function has the same form as that for a monatomic gas, the difference being the additional degrees of freedom (vibrational and rotational) that arise in the diatomic molecule which must be accounted for. The most general form of the diatomic partition function, Z_d, has the same form as that of the monatomic gas:

$$Z_d(T,V,N_g) = \frac{z_d(T,V)^{N_g}}{N_g!} \quad (3.8)$$

The additional degrees of freedom are included in the term z_d, which can be expanded as [Kub65]:

$$z_d = z_g \times z_{vib} \times z_{rot} \quad (3.9)$$

where z_g is the same as in Eq. 3.6, the vibrational term with vibrational frequency ν is:

$$z_{vib} = \left[2sinh\frac{\theta_v}{2T}\right]^{-1} (\theta_v = h\nu/k_B) \quad (3.10)$$

and the rotational term:

$$z_{rot} = \frac{8\pi^2 I}{h^2\beta} \quad (3.11)$$

Debye model of solid

When choosing a model for the solid partition function the Einstein and Debye models were two possible choices. The Debye model was chosen over the Einstein model because it is known to be more accurate in predicting properties of a solid that are dependent on lattice vibrations. The Einstein model assumes that each atom is three linear independent oscillators. These oscillators are assumed to vibrate with a single frequency and this is the main draw back of the Einstein model. With the Debye model phonons were used to explain vibrations of the lattice rather than treating each atom independently. Also in the Debye model there is a range of frequencies, ω to $\omega + d\omega$, that are allowed.

Debye frequency

The minimum frequency in the Debye model is typically taken to be zero to correspond to infinite wave length, and the maximum is known as the Debye frequency, ω_D. The Debye frequency corresponds to wave lengths that are on the order of several lattice spacings. At low frequencies the Debye model assumes a linear dispersion relation between the frequency and the wave number, k.

$$\omega = vk \tag{3.12}$$

Where the slope is the velocity of sound waves in the material, v. There are two possible types of waves, longitudinal and transverse, which travel at different velocities and need to be accounted for. At high frequencies the dispersion curves deviate from the linear relation and flatten out. To use the Debye model it was necessary to calculate the Debye frequency for each material, this can be done by using the linear relationship between frequency and the wave number. The following equation, which is equivalent to the density of states in the frequency

range $d\omega$, can be used to determine the Debye frequency [Cal60]:

$$D(\omega) = \frac{V}{2\pi^2} k^2(\omega) \frac{dk(\omega)}{d\omega} d\omega \tag{3.13}$$

V is the volume, here the unit cell volume was used, and $k(\omega)$ is taken by solving Eq. 3.12 for k. After doing so and accounting for the one longitudinal mode with velocity v_l and two transverse modes with velocity v_t, Eq. 3.13 becomes:

$$D(\omega) = \frac{V}{2\pi^2} \left(\frac{1}{v_l^3} + \frac{2}{v_t^3} \right)^{-1} d\omega \tag{3.14}$$

By integrating Eq. 3.14 over possible frequencies, and using the fact that this must be equal to the total number of modes, $3N$, the Debye frequency can be found:

$$\int_0^{\omega_D} D(\omega) d\omega = 3N \tag{3.15}$$

$$\omega_D^3 = \frac{18N\pi^2}{V} \left(\frac{1}{v_l^3} + \frac{2}{v_t^3} \right)^{-1} \tag{3.16}$$

To use Eq. 3.16 the longitudinal and transverse wave velocities of the solids needed to be determined. The following relation, between the elastic constant c_{ij} and material denisty ρ, can be used to calculate the velocities:

$$v = \sqrt{\frac{c_{ij}}{\rho}} \tag{3.17}$$

Use of this equation allows for the calculation of the Debye frequency to be made using *ab inito* methods, which are capable of calculating elastic constants of materials. The longitudinal and transverse velocities are dependent on crystal structure, which determine which elastic constant to be used for each velocity [Pol77]. For a hexagonal material (e.g. Zn) the longitudinal and transverse velocities are:

$$v_l^{hex} = \sqrt{\frac{c_{33}}{\rho}} \tag{3.18}$$

$$v_t^{hex} = \sqrt{\frac{c_{44}}{\rho}} \tag{3.19}$$

and for cubic materials (e.g. Sn, Ge):

$$v_l^{cub} = \sqrt{\frac{c_{11}}{\rho}} \tag{3.20}$$

$$v_t^{cub} = \sqrt{\frac{c_{44}}{\rho}} \tag{3.21}$$

The velocities are also dependent on crystal direction and for both cases the [100] direction was chosen. The elastic constants can be predicted fairly reliably using density functional theory.

Solid partition function

The partition function of a solid can be factored into a term that corresponds to a material with no phonons and into one containing the effects of phonons [Kub65]. In a solid with no phonons the energy contribution is η (the binding energy per atom at absolute zero), which can be calculated from total energy calculations using density functional theory. There is some error in density functional theory when using the LDA due to the well known over binding, but the total energy is fairly accurate and improvements can be made by using the Perdew-Burke-Ernzerhof (PBE) functional. The contribution from a solid without phonons is simply:

$$z_s = e^{-\eta\beta N_s} \tag{3.22}$$

The contribution due to phonons was then determined by using the Debye model of a solid. This can be done by starting from the partition function for a harmonic oscillator with angular frequency ω_j:

$$Z_j = \sum_{n=0}^{\infty} e^{-\left(n+\frac{1}{2}\right)\hbar\omega_j\beta} = \left[1 - e^{-\hbar\omega_j\beta}\right]^{-1} \tag{3.23}$$

The total partition function due to phonons in the solid then becomes:

$$z_{phonon} = \prod_j Z_j = \prod_j \left[1 - e^{-\hbar\omega_j\beta}\right]^{-1} \tag{3.24}$$

By combining the contributions from the solid with and without phonons the total Debye solid partition function is:

$$Z_s(T, N_s) = z_s \times z_{phonon} = e^{-\eta N_s \beta} \prod_j \left[1 - e^{-\hbar\omega_j\beta}\right]^{-1} \tag{3.25}$$

With appropriate partition functions for the solid and gas phases the free energy can be determined, and the number of atoms in the gas phase can be found satisfying the conditions for chemical equilibrium.

3.3 Single component system: Zn, Ge, Sn

The simplest case for the calculation of the vapor pressure over a solid is that of a single component system that exists in a single phase solid and a monatomic gas phase. Here three different solids were studied; zinc, tin, and germanium. Each system can be described by the same chemical reaction, $M(s) \rightarrow M(g)$, the decomposition of the solid to the gas phase. This forward reaction will dominate until there is a sufficient number of atoms in the gas phase colliding with the solid such that there is a net flux of zero atoms leaving the solid. Using Eq. 1.18, the condition for equilibrium of a single component system can be written as:

$$\mu_g - \mu_s = 0 \tag{3.26}$$

where s and g represent the solid and gas phases respectively. This leads to the following equation which must be solved for the number of atoms in the gas phase:

$$\frac{\partial lnZ_g(T, V, N_g)}{\partial N_g} = \frac{\partial lnZ_s(T, N_s)}{\partial N_s} \tag{3.27}$$

After using Eq. 3.7 and applying Stirling's approximation for the natural logarithm of a factorial the result of differentiating the left hand side of Eq. 3.39 is:

$$\frac{\partial lnZ_g(T, V, N_g)}{\partial N_g} = lnN_g - lnz_g(T, V) \tag{3.28}$$

The result from the right hand side of Eq. 3.39 using the solid partition function in Eq. 3.25 is:

$$\frac{\partial lnZ_s(T,N_s)}{\partial N_s} = \left[-\eta\beta - \frac{9}{\omega_D}\int_0^{\omega_D} ln\left[1-e^{-\hbar\omega_j\beta}\right]\omega^2 d\omega\right] = \beta\mu_s \tag{3.29}$$

the complete derivation of Eq. 3.41 can be found in appendix A. By equating Eqs. 3.40 and 3.41, the number of atoms in the gas phase can be solved for:

$$N_g(T) = z_g(T,V)e^{-\beta\mu_s} \tag{3.30}$$

It was chosen to not solve the integral contained in Eq. 3.45 analytically, but to instead solve it numerically when calculating the number of atoms in the gas phase as a function of temperature. Having derived an equation for the number of atoms in the gas phase the pressure due to the gas can be calculated using the ideal gas law.

3.4 Binary system: GaAs

For a binary system, the same basic steps are followed as in the single component system. However, complexities arise in that there can now be multiple solid phases as well as multiple species in the gas phase. The decomposition of GaAs was studied as an example binary system. The major complications that arise from this simple binary system include: arsenic forms a diatomic gas, gallium could decompose from GaAs as either a solid or gas, and GaAs forms a zincblend solid phase only when the ratio of Ga to As is unity [Tsa93]. To simplify the system it was chosen here that the solid would decompose into a vapor with same composition as the solid, or:

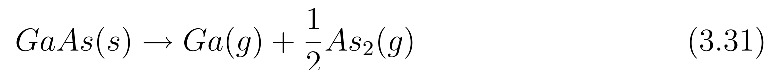

$$GaAs(s) \rightarrow Ga(g) + \frac{1}{2}As_2(g) \tag{3.31}$$

which leads to the equilibrium condition:

$$\mu_{Ga} + \frac{1}{2}\mu_{As_2} - \mu_{GaAs} = 0 \tag{3.32}$$

The equilibrium condition can also be written as:

$$lnN_{As_2} + 2lnN_{Ga} = lnz_{As_2}(T,V) + 2lnz_{Ga}(T,V) - 2\beta\mu_{GaAs} \tag{3.33}$$

This equation however contains two unknowns, the number of arsenic and gallium atoms in the gas phase. Since it was assumed that the composition of the gas phase would be the same as the solid, the number of gallium atoms in the gas phase must then be $N_{Ga} = 2N_{As_2}$. The number of arsenic molecules in the gas phase can now be calculated using the following equation:

$$N_{As_2} = 2\sqrt{z_{As_2}(T,V)z_{Ga}(T,V)e^{-2\beta\mu_{GaAs}}} \tag{3.34}$$

The vapor pressure of arsenic over GaAs can then be calculated using Eq. 3.34 for the number of arsenic molecules, and the ideal gas law for the corresponding pressure.

3.5 Ternary system: $ZnGeAs_2$

To calculate the vapor pressure over $ZnGeAs_2$, it was assumed that only mechanism for atoms to enter the gas phase from the solid was by the formation of vacancies described by the following reactions:

$$Zn^x_{Zn} \rightarrow V^x_{Zn} + Zn(g) \tag{3.35}$$

$$Ge^x_{Ge} \rightarrow V^x_{Ge} + Ge(g) \tag{3.36}$$

$$As^x_{As} \rightarrow V^x_{As} + \frac{1}{2}As_2(g) \tag{3.37}$$

Since it was assumed that vacancies are the only allowed defect, each species could only exist in two different states, either on its correct lattice site or in the gas phase. To determine the vapor pressure the number of atoms in the gas phase was calculated by minimizing the free energy of the system with respect to the number of atoms in each phase. Even with this over simplification of allowing vacancies to be the only defect present in the material, this assumption produces a rather accurate prediction of the vapor pressure.

Using Eqs. 3.7 and 3.25, the total free energy of the system can be written as:

$$F(T,V,N) = -k_B T\left[lnZ_g(T,V,N_{Zn},N_{Ge},N_{As_2}) + lnZ_s(T,N_{Zn},N_{Ge},N_{As})\right]^{1} \tag{3.38}$$

In an attempt to simplify the problem, an additional assumption as made that the decomposition of the solid would occur stoichiometrically, i.e. $N_{Zn} = N_{Ge} = N_{As_2}$ in the gas phase. This allows for the replacement of each atom number by a single variable, N_g. The same can be also done for the solid, where the individual N_i can bet set to N_s. To determine the equilibrium number of atoms in the gas phase the free energy of the system must be minimized with respect to the number of atoms in the gas phase:

$$\frac{\partial lnZ_g(T,V,N_g)}{\partial N_g} = \frac{\partial lnZ_s(T,N_s)}{\partial N_s} \tag{3.39}$$

After using Eq. 3.7 and applying Stirling's approximation for the natural logarithm of a factorial the result of differentiating the left hand side of Eq. 3.39 is:

$$\frac{\partial lnZ_g(T,V,N_g)}{\partial N_g} = lnZ_g^{Zn}(T,V,N_{Zn})Z_g^{Ge}(T,V,N_{Ge})Z_d^{As_2}(T,V,N_{As_2})^{1/2} - lnN_g^{5/2} \tag{3.40}$$

The result from the right hand side of Eq. 3.39 using the solid partition function in Eq. 3.25 is:

$$\frac{\partial lnZ_s(T,N_s)}{\partial N_s} = \left[-\eta\beta - \frac{3\times 9}{\omega_D}\int_0^{\omega_D} ln\left[1-e^{-\hbar\omega_j\beta}\right]\omega^2 d\omega\right] = \beta\mu_s \tag{3.41}$$

where

$$\eta = \eta_{V_{Zn}} + \eta_{V_{Ge}} + \eta_{V_{As}} \tag{3.42}$$

[1] Take note that N_i in the gas and solid partition functions are not assumed to be equal

With η being the defect formation energy of a neutral (q=0) defect α in $ZnGeAs_2$ which is dependent on the chemical potentials [ZWZKY98]:

$$\eta(\alpha, q = 0) = \Delta E(\alpha, q = 0) + n_{Zn}\mu_{Zn} + n_{Ge}\mu_{Ge} + n_{As}\mu_{As} \tag{3.43}$$

where

$$\Delta E(\alpha, q = 0) = E(\alpha, q = 0) - E(ZnGeAs_2) + n_{Zn}\mu^{solid}_{Zn} + n_{Ge}\mu^{solid}_{Ge} + n_{As}\mu^{solid}_{As} \tag{3.44}$$

In Eq. 3.43, n_i are the atomic species that either added or removed from the systems, and μ_i are the chemical potentials of the atomic species, which are controlled by laboratory conditions (pressure and temperature). Eq. 3.44 is the expression for the difference in energy between the defect cell ($E(\alpha, q = 0)$) and the perfect cell ($E(ZnGeAs_2)$). These energies are obtained from density functional theory calculations (DFT) of fully relaxed supercells. The n_i terms are the same as in Eq. 3.43, the solid chemical potentials, μ^{solid}_i, are the total energies of the elemental solids, which are also obtained from DFT calculations.

After setting the two sides equal and solving for N_g one finds the number of atoms in the gas phase is:

$$N_g(T) = \left[(Z^{Zn}_g(T, V)Z^{Ge}_g(T, V)Z^{As_2}_d(T, V)^{1/2})^{-1}e^{-\beta\mu_s}\right]^{-2/5} \tag{3.45}$$

By then using the ideal gas law, the vapor pressure can now be found:

$$P(T) = k_bT\left[(Z^{Zn}_g(T)Z^{Ge}_g(T)Z^{As_2}_d(T)^{1/2})^{-1}e^{-\beta\mu_s}\right]^{-2/5} \tag{3.46}$$

The volume dependence is canceled out when the ideal gas law is substituted in for $N_g = PV/k_BT$.

3.6 Results and Discussion

Monatomic Systems: Zn, Ge, Sn

The vapor pressures for the three materials studied was calculated using basic materials properties (mass, density, and unit cell volumes), properties calculated from

ab initio electronic structure methods (total energies), and data from literature (elastic constants). The materials data used for the vapor pressure calculations, along with parameters calculated during the process can be found in table 3.1.

Table 3.1: Materials data used for calculation of Zn, Ge, and Sn vapor pressures

	From Literature [Nye57, Ada04]		Calculated	
Zn	c_{33}	6.29×10^{10} $[Nm^{-2}]$	v_l	2.99×10^{3} $[m\ s^{-1}]$
	c_{44}	3.79×10^{10} $[Nm^{-2}]$	v_t	2.32×10^{3} $[m\ s^{-1}]$
	m	1.07×10^{-25} $[kg]$	ω_D	1.65×10^{13} $[rad\ s^{-1}]$
	ρ	7.04×10^{3} $[kg\ m^{-3}]$	ϕ_{LDA}	-1.847 $[eV]$
	V_{cell}	2.00×10^{-28} $[m^{3}]$	ϕ_{PBE}	-1.095 $[eV]$
Sn	c_{11}	6.90×10^{10} $[Nm^{-2}]$	v_l	3.46×10^{3} $[m\ s^{-1}]$
	c_{44}	3.62×10^{10} $[Nm^{-2}]$	v_t	2.50×10^{3} $[m\ s^{-1}]$
	m	1.97×10^{-25} $[kg]$	ω_D	1.37×10^{13} $[rad\ s^{-1}]$
	ρ	5.77×10^{3} $[kg\ m^{-3}]$	ϕ_{LDA}	-3.835 $[eV]$
	V_{cell}	4.59×10^{-28} $[m^{3}]$	ϕ_{PBE}	-3.143 $[eV]$
Ge	c_{11}	12.87×10^{10} $[Nm^{-2}]$	v_l	4.92×10^{3} $[m\ s^{-1}]$
	c_{44}	6.67×10^{10} $[Nm^{-2}]$	v_t	3.54×10^{3} $[m\ s^{-1}]$
	m	1.21×10^{-25} $[kg]$	ω_D	2.22×10^{13} $[rad\ s^{-1}]$
	ρ	5.33×10^{3} $[kg\ m^{-3}]$	ϕ_{LDA}	-4.468 $[eV]$
	V_{cell}	3.03×10^{-28} $[m^{3}]$	ϕ_{PBE}	-3.747 $[eV]$

The resulting vapor pressure calculations using the data in Table 3.1 are displayed in figure 3.1. It can be seen in the figure that for each element the fit using the LDA total energy falls below the experimental data [Mar67]. Each fit however appears to have the correct trend in comparison with the data, this indicated that the model was correct and that it was possibly the data being used that was incorrect. The only values that were not basic materials properties pulled from literature were the LDA energies and the Debye frequency. After comparing the calculated wave velocities and Debye frequencies with literature [Ada04] it was apparent that they were fairly accurate. This left the LDA energies as the possible source of error. It is known that the LDA produces errors in total energy calculations due to over binding. To calculate more accurate total energies, the calculations were redone, using the Perdew-Berke-Ernzerhof (PBE) functional

[PBE96]. The resulting vapor pressures using the PBE functional in the total energy calculations is plotted along with the LDA results, and it can be seen that they agree much better with experimental data.

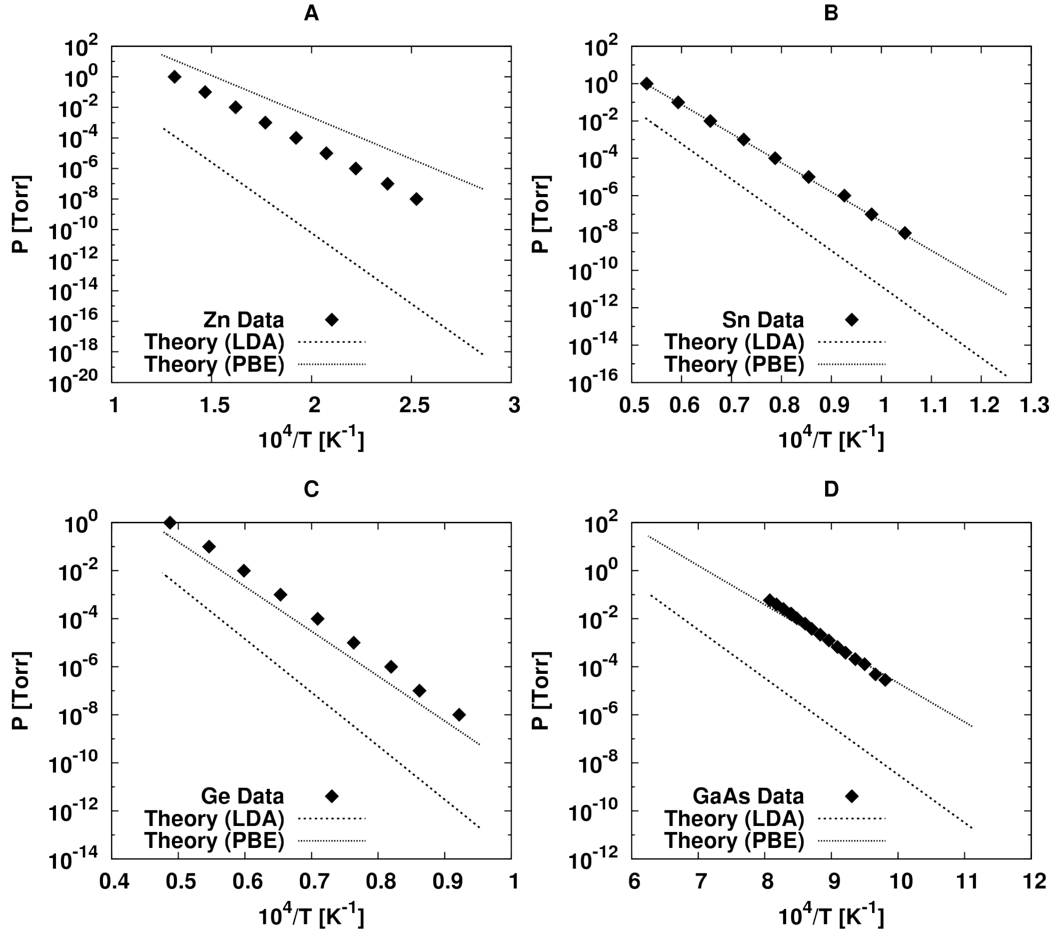

Figure 3.1: Arrhenius plots of the comparison between experimental data [Mar67] and theory (LDA and PBE calculations) for the monatomic systems A) Zn, B) Sn, C) Ge, and the binary system D) GaAs

The results from the monatomic systems appear to validate the methods used for these systems, and also show that the total energy calculations should be performed using the PBE functional. The following section describes the results from the version of this method adapted for binary systems.

Transition from the monatomic to binary system was fairly straight forward, the main difference was the additional agree of freedom according to Gibbs's phase rule. This additional degree of freedom is the partial pressure of the gas phase for Ga and As_2. It was found that for the theory to agree with the experimental data the partial pressures had to reflect the stoichiometry of the solid, in this case 1:1. The data used for these calculations can be found in Table 3.2.

Table 3.2: Materials data used for calculations of GaAs vapor pressure

	From Literature [Ada04]		Calculated	
GaAs	c_{11}	1.19×10^{11} $[Nm^{-2}]$	v_l	4.73×10^3 $[m\ s^{-1}]$
	c_{44}	0.60×10^{11} $[Nm^{-2}]$	v_t	3.36×10^3 $[m\ s^{-1}]$
	m	2.40×10^{-25} $[kg]$	ω_D	2.40×10^{13} $[rad\ s^{-1}]$
	ρ	5.316×10^3 $[kg\ m^{-3}]$	ϕ_{LDA}	-3.920 $[eV]$
	V_{cell}	1.78×10^{-28} $[m^3]$	ϕ_{PBE}	-3.163 $[eV]$

As in the monatomic systems it was found that the LDA total energies resulting in vapor pressures that were several order of magnitude lower than experimental data. Once PBE total energies were used the resulting theoretical vapor pressure again agreed very well with experiment, as show in Fig. 3.1. It was found that the main adjustments that needed to be made to predict the vapor press over a binary compound was how to handle the additional degree of freedom, and making sure to account for the diatomic gas as described in the methods. As stated the additional degree of freedom, the gas partial pressures, was chosen to reflect the stoichiometry of the film. The diatomic gas is not specifically related to the binary system, but it is to GaAs and will most likely be present with $ZnGeAs_2$ as well.

Similar to transitioning from the monatomic to binary system, the transition from binary to ternary meant that another degree of freedom was added to the system. The main difficulty with this was to determine what the final state of the system should be. With $ZnGeAs_2$ consisting of 3 components, there was the simplest case where each component simply evaporated from the solid to a gas, or something more complex involving additional solid phases. It turned out though that the simplest system appears to agree best with experimental data – each species evaporating to a gas phase with no additional solid phases. The main difference though that had to be accounted for was the difference in formation energies of the three vacancies.

In the monatomic systems one simply only needs the heat of formation for the solid to calculate the vapor pressure. Similarly in GaAs, since it is well known that if one species evaporates the other will also evaporate, thus allowing for the heat of formation to be used as the activation energy in the vapor pressure calculation. However, in $ZnGeAs_2$ the vacancy formation energy of each species ranges from Zn having the lowest, to Ge having the largest, mostly due to the contribution from solid Ge which must be accounted for in the defect formation energy (Eq. 3.44).

The resulting vapor pressure for $ZnGeAs_2$ is displayed in Fig. 3.2, which is plotted alongside experimental data and the theoretical Zn vapor pressure from Fig. 3.1. In comparison to the experimental results for sputtering [SG84], MBE [STP89], and the decomposition data [VTT+11] it would appear that the vapor pressure calculated here is too high. The explanation for this is that it has been proposed there is a kinetic barrier to thermal decomposition of $ZnGeAs_2$

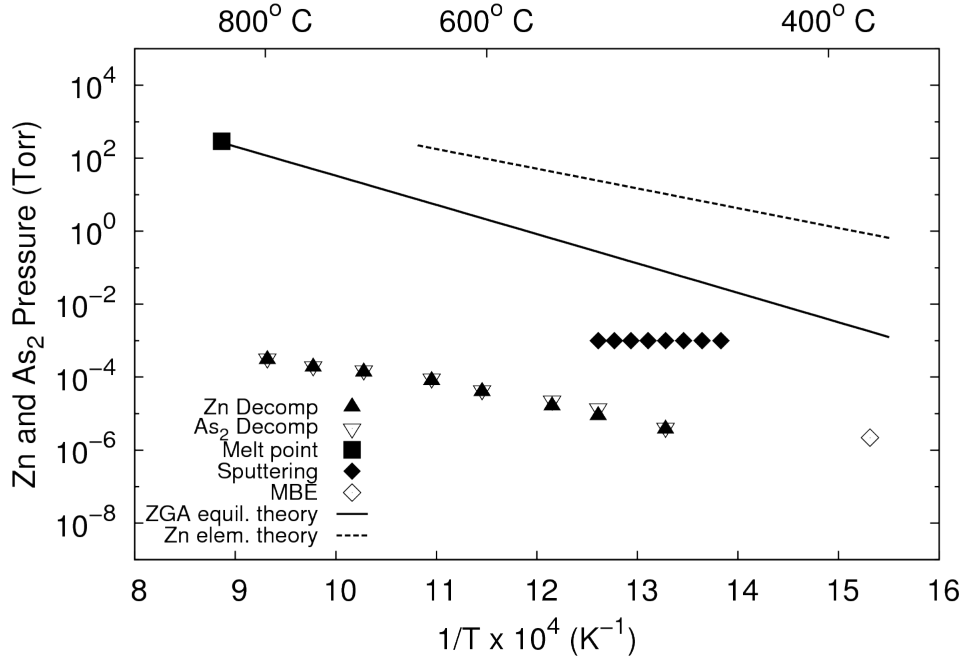

Figure 3.2: Arrhenius plot of the vapor pressure over ZGA in comparison to thermal decomposition data, the vapor pressure over liquid ZGA at the melting point [SW75], and arrival rates for Zn and As via sputtering [SG84] and As via MBE synthesis [STP89]

[VTT+11]. This would explain the ability for growth below the theoretical vapor pressure, which seems to occur in a meta-stable region. This is claim is further validated from the vapor pressure over $ZnGeAs_2$ at the melting point [SW75], which is a better representation of the thermodynamical limit of the vapor pressure, which falls almost perfectly on the theoretical vapor pressure calculated here. Since the methods followed here were based in thermodynamic theory, it is not possible to predict kinetically limited reactions with these methods. Similar kinetic barriers are found in GaN [New97] which is a material that is strongly bonded like $ZnGeAs_2$, so it is very possible for there to be strong kinetic barriers present in $ZnGeAs_2$.

3.7 Conclusions

In conclusion, it has been shown that the theoretical vapor pressure of a ternary compound (e.g. $ZnGeAs_2$) can be calculated from first principles. This was accomplished using methods adapted from statistical mechanics to predict the vapor pressure over a monatomic solid [Kub65]. Once these methods were validated (Fig. 3.1) using experimental data available for Zn, Ge, and Sn it was when adapted for use with the binary compound GaAs. In the adaptation to a binary system it was discovered that the additional degree of freedom was best chosen such that the gas would retain the same stoichiometry of the solid. The adapted binary method was also successful in predicting the vapor pressure of the GaAs system with good accuracy (Fig. 3.1).

With a validated method for monatomic and binary systems it was then possible to make the additional changes to predict ternary systems. Similar to GaAs it was found that the gas should keep the same stoichiometry of the film to predict the vapor pressure over a stoichiometric film. It was also discovered that the formation energy for each of the three vacancies must be accounted for an accurate prediction. Comparison of the theoretical vapor pressure predicted here for $ZnGeAs_2$ (Fig. 3.2) suggests that there are strong kinetic barriers to the thermal decomposition of the material.

Chapter 4

Summary

4.1 Native Point Defects in $ZnGeAs_2$

In summary, methods for the calculation of defect formation energies and the prediction of defect concentrations have been shown. In calculating the defect formation energies of native point defects in $ZnGeAs_2$ a stability diagram was also created from the limits imposed on chemical potentials of the various species. From this the range of chemical potentials to focus on the ranges that would translate to typical growth conditions. Using the range of chemical potentials gained from the stability diagram the formation energy for the two cation vacancies and anti-sites was calculated and plotted. From this it was shown that the zinc vacancy (V_{Zn}) and the germanium anti-site (Ge_{Zn}) have the lowest formation energies, and should therefor be the most abundant.

To gain a better idea of the abundance of these defects the concentrations for the three vacancies (Zn, Ge, and As) and two anti-sites (Ge_{Zn} and Zn_{Ge}) were calculated. These were thought to be the most likely to contribute to forming off-stoichiometry films, and it was found that under typical growth conditions the zinc vacancy (V_{Zn}) and the germanium anti-site (Ge_{Zn}), would be the most abundant, as predicted from their formation energies. While it appears that under normal growth conditions it may be difficult to limit their formation, the information gathered here could be used to formulate annealing procedures to reduce the native defects in as-grown films. To gain additional knowledge of the defect physics occurring in $ZnGeAs_2$ it would be useful to perform these calculations for ionized defects to gain information for n/p-type doping as well as the possibility of defect complexes that may form.

4.2 *ab initio* Vapor Pressure Model

In summary, it has been shown that the theoretical vapor pressure of a ternary compound (e.g. $ZnGeAs_2$) can be calculated from first principles. This was accomplished using methods adapted from statistical mechanics to predict the vapor pressure over a monatomic solid [Kub65]. Once these methods were validated (Fig. 3.1) using experimental data available for Zn, Ge, and Sn it was when adapted for use with the binary compound GaAs. In the adaptation to a binary system it was discovered that the additional degree of freedom was best chosen such that the gas would retain the same stoichiometry of the solid. The adapted binary method was also successful in predicting the vapor pressure of the GaAs system with good accuracy (Fig. 3.1).

With a validated method for monatomic and binary systems it was then possible to make the additional changes to predict ternary systems. Similar to GaAs it was found that the gas should keep the same stoichiometry of the film to predict the vapor pressure over a stoichiometric film. It was also discovered that the formation energy for each of the three vacancies must be accounted for an accurate prediction. Comparison of the theoretical vapor pressure predicted here for $ZnGeAs_2$ (Fig. 3.2) suggests that there are strong kinetic barriers to the thermal decomposition of the material.

[Ada04] S. Adachi, *Handbook on physical properties of semiconductors*, vol. 1, Kluwer, 2004.

[BvSS94] M. A. Berding, M. van Schilfgaarde, and A. Sher, *First-principles calcualtion of native defects densities in $hg_{0.8}cd_{0.2}te$*, Physical Review B **50** (1994), no. 3.

[Cal60] H. B. Callen, *Thermodynamics and an introduction to thermostatistics*, Wiley, 1960.

[CCO+87] B. Chelluri, T.Y. Chang, A. Ourmazd, A.H. Dayem, J.L. Zyskind, and A. Srivastava, *Molecular beam epitaxial growth of ii–v semiconductor zn3as2 and ii–iv–v chalcopyrite zngeas2*, Journal of Crystal Growth **81** (1987), no. 1-4, 530–535.

[HK64] P. Hohenberg and W. Kohn, *Inhomogeneous electron gas*, Physical Review **136** (1964), no. 3B.

[JML05] Xiaoshu Jiang, M. S. Miao, and Walter R. L. Lambrecht, *Theoretical study of cation-related point defects in $zngep_2$*, Physical Review B **71** (2005), no. 205212.

[Kro74] F. A. Kroger, *The chemistry of imperfect crystals*, 2 ed., vol. 2, North-Holland, 1974.

[KS65] W. Kohn and L. J. Sham, *Self-consistent equations including exchange and correlation effects*, Physical Review **140** (1965), no. 4A.

[Kub65] R. Kubo, *Statistical mechanics*, El Sevier, 1965.

[Mar67] J. Margrave (ed.), *The characterization of high temperature vapors*, Wiley, 1967.

[MvSC00] M. Methfessel, M. van Schilfgaarde, and R. A. Casali, *A full-potential lmto method based on smooth hankel functions*, Electronic Stucture and Physical Properties of Solids (Hugue Dreyssé, ed.), Lecture Notes in Physics, vol. 535, Springer, 2000.

[New97] N. Newman, *The energetics of the gan mbe reation: a case study of meta-stable growth*, Journal of Crystal Growth **178** (1997), 102–112.

[Nye57] J. F. Nye, *Physical properties of crystals*, Oxford: Clarendon Press, 1957.

[PBE96] John P. Perdew, Kieron Burke, and Matthias Ernzerhof, *Generalized gradient approximation made simple*, Physical Review Letters **77** (1996), no. 18.

[Pol77] H. F. Pollard, *Sound waves in solids*, Pion, 1977.

[PY89] Robert G. Parr and Weitao Yang, *Density-functional theory of atoms and molecules*, Oxford University Press, 1989.

[Rei65] F. Reif, *Fundamentals of statistical and thermal physics*, McGraw-Hill, 1965.

[SG84] S.I. Shah and J.E. Greene, *Growth and physical properties of amorphous and single crystal zngeas2 layers deposited on (100)gaas by*

sputter deposition in excess zn and as4, Journal of Crystal Growth **68** (1984), no. 2, 537–544.

[STP89] G.S. Solomon, M.L. Timmons, and J.B. Posthill, *Organometallic vapor phase epitaxial growth and characterization of zngeas2 on gaas*, Journal of Applied Physics **65** (1989), no. 5, 1952.

[SW75] J.L. Shay and J. Wernick, *Ternary chalcopyrite semiconductors: growth, electronic properties and applications*, Pergamon New York, 1975.

[TB98] M.L. Timmons and K.J. Bachmann, *Growth of nlo chalcopyrite materials by omvpe*, Mat. Res. Soc. Symp. Proc. **484** (1998), 507.

[Tsa93] J. Y. Tsao, *Materials fundamentals of molecular beam eitaxy*, Academic Press, 1993.

[VTT+11] M. Vahidi, Z.Z. Tang, J. Tucker, T.J. Peshek, C. Kopas, R.K. Singh, M. van Schilfgaarde, and N. Newman, *Experimental study of the kinetically-limited decomposition of zngeas$_2$ and its role in determine optimal conditions for thin film growth*, Submitted to Acta Materialia July 2011, 2011.

[ZWZKY98] S.B. Zhang, Su-Huai Wei, Alex Zunger, and H. Katayama-Yoshida, *Defect physics of the cuinse$_2$ chalcopyrite semicondutor*, Physical Review B **57** (1998), no. 16.

Appendix A

Differentiation of Solid Partition Function

Starting from Eq. 3.25 and taking the natural logarithm of a product can be rewritten as a sum of the natural logarithm:

$$lnZ_s(T, N_s) = -\eta N_s \beta - \sum_j ln\left[1 - e^{-\hbar\omega_j\beta}\right] \tag{A.1}$$

The sum can then be changed to an integral over the frequency range, $d\omega$, by the addition of a function describing the distribution of states. By combining Eqs. 3.14 and 3.16 the distribution of states can be determined as a function of frequency, number of atoms, and the Debye frequency. After the addition of the frequency distribution Eq. A.1 can now be written as:

$$lnZ_s(T, N_s) = -\eta N_s \beta - \int_0^{\omega_D} ln\left[1 - e^{-\hbar\omega_j\beta}\right] \frac{9N_s}{\omega_D^3}\omega^2 d\omega \tag{A.2}$$

The $9N_s/\omega_D^3$ term can be pulled out of the integral and the result is:

$$lnZ_s(T, N_s) = \frac{-\eta N_s \beta}{k_B T} - \frac{9N_s}{\omega_D^3} \int_0^{\omega_D} ln\left[1 - e^{-\hbar\omega_j\beta}\right] \omega^2 d\omega \tag{A.3}$$

This equation can now be easily differentiated with respect to the number of atoms, and upon doing so:

$$\frac{\partial lnZ_s(T, N_s)}{\partial N_s} = \left[-\eta\beta - \frac{9}{\omega_D} \int_0^{\omega_D} ln\left[1 - e^{-\hbar\omega_j\beta}\right] \omega^2 d\omega\right] \tag{A.4}$$